International Journal of Computing and Digital Systems
ISSN (2210-142X)
Int. J. Com. Dig. Sys. 12, No.1 (Oct-2022)

https://dx.doi.org/10.12785/ijcds/120190

A New Synthetic Aperture Radar (SAR) Image Classification Framework Model using SAR Despeckling

Bibek Kumar[1], Ranjeet Kumar Ranjan[1] and Arshad Husain[1]

[1]*School of Computing, DIT University,Dehradun, Uttarakhand, India*

Received 22 Jan. 2021, Revised 15 Jul. 2022, Accepted 23 Jul. 2022, Published 31 Oct. 2022

Abstract: In recent years, the popularity of the synthetic aperture radar (SAR) imaging system is growing exponentially. The SAR images are mainly used for the identification or classification of objects for various purposes. The classification of objects from SAR images can be difficult due to the multiplicative noise present in the images and the high dimensionality. In this manuscript, a machine learning based approach to classify images labeled with multiple classes has been proposed. Proposed approach first deals with speckling the images using a multi-objective enhanced Fruit Fly optimization method. Next, it applies a principal component analysis-based method for feature extraction. Finally, the despeckled and extracted features are used to evaluate the Support Vector Machine classifier. The proposed approach has performed well with the training and testing accuracy of 99.73% and 98.10% respectively. The experiments show that the despeckling has improved the performance of the proposed classifier to a great extent. The proposed approach also performed better than some other machine learning classifiers as well as some existing literature in terms of different performance measures.

Keywords: Remote Sensing, SAR Despeckling, SAR Classification, Machine Learning, Support Vector Machine

1. Introduction

Remote sensing is a field of gathering data of any targeted earth surface from a large distance. In the process of gathering data, satellites or aircrafts are used to record and save reflected energy via remote sensors. The reflected energy is also known as echo. Amplitude and phase of the received echo in coherent SAR systems, is used in the converging process to construct the image. This captured data can be restored through digital and analog methods. The digital method is much easier than the analog method because of radar receiver whereby storing of data involved [1]. The collected image data can be used to identify and classify the objects of the targeted surface area. There are two kinds of sensors which can be used to capture the image data; the first is active sensors and the second is known as passive sensors. The active sensors generate their own energy and internment reflected energy from the targeted surface. The advantage of capturing data through active sensors, such as SAR images, are not affected by time intervals and weather conditions. Therefore, SAR datasets are used frequently in different generous of analysis including geography, earth observation, agriculture, military war, oceanography, and disaster management. Passive remote sensing incorporates a different kind of radiometer, unlike active remote sensing as shown in Figure 1. Typically, passive sensors used solar energy as an energy source and gathered reflected electromagnetic energy [2].

Remote sensing methods are typically classified into two major categories. The first method is optical remote sensing, which uses optical sensors of satellites to capture the targets by noticing the reflected wave from the target. The second method of remote sensing is infrared remote sensing, in which satellite's infrared sensors are used to determine infrared radiated waves from the target. The electromagnetic signals received by the sensor are used to form an image with the help of various wavelengths. Spectral signature of targets is formed with the help of various wavelength bands of solar radiation reflected from the target. Spectral signature is known as the deviation of emittance or reflectance of a material with respect to wavelengths.

These satellite images are generally classified into three key categories depending upon the used spectral band of the imaging system. The first category is the panchromatic image which uses the entire wavelength as a single spectral band. The second category is multispectral images, which uses 3-15 spectral bands included both color and brightness information of target, and the last one is the hyperspectral image, which uses hundreds of spectral bands with a narrow bandwidth (5-10nm). These hyperspectral images give precise spectral information,which could be utilized for better characterization and detection of objects into the image.

E-mail address: bkknith@gmail.com, ranjeetghitm@gmail.com, arshad.husain18@gmail.com

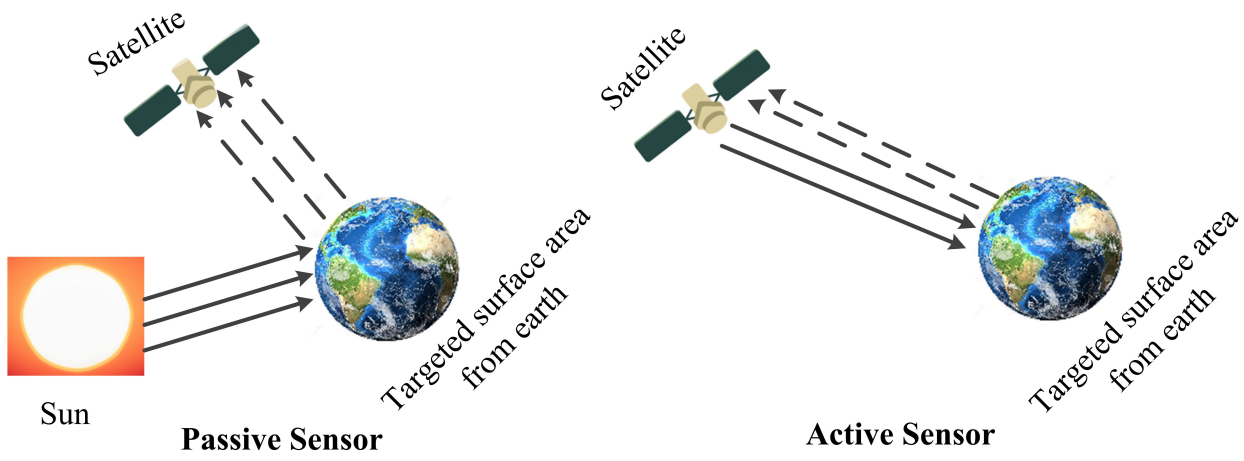

Figure 1. Capturing process by passive and active sensors

The resolution of these captured images is categorized into four measures. The first measure is radiometric resolution, which can be measured by the quantity of information in each pixel spatial resolution represents by size of every pixel. The spectral resolution represents the ability of a sensor to determine the clearer wavelength and temporal resolution means the time taken by the satellite to re-examine the same targeted area. Once data is collected then it is processed and made ready to use for analysis [3].

The spatial resolution of radar statistics is strongly linked with the proportion of the sensor wavelength and the size of the sensor's antenna. Therefore, the higher sensor's antenna length produced a high resolution of the images for a given wavelength.

SAR images are originated from the moving satellite or aircraft and due to the height of the sensor's antenna, the resolution of the images becomes very high. The structures of these captured SAR images are called single look complex (SLC) and termed by the multiplicative noise of speckle noise. To reduce the effect of multiplicative noise and reduce resolution of the images, a multi looking method are used on the SLC images, and it improved the quality of SAR image by squaring the pixel value [4]. The high resolution and presence of multiplicative noise makes very tedious challenges for analysis to classify images.

The old technique of classification was used to obtain some handmade features and train a classifier [5], [6]. A backscattering and geometrical characteristics-based classification architecture was proposed [7]. In this architecture, authors have analyzed the backscattered and geometrical features of cargo ships and classified into the oil tankers, containers ship and bulk carriers. An azimuth sensitivity information (ASI) based method was introduced [8] in which original SAR images based ASI was created, and it used the azimuth sensitivity of any particular target class at any specific azimuth. Another improved shape context method was introduced [9], which illustrate the topology and scattering points intensity in the target. In all these methods, researchers are required to design features, which have some demerits such as features that need to be changed as per the target and zero or lack of knowledge about the best features to train a model.

With the advancement of machine learning and deep learning techniques, there are many object recognition fields performed well such as convolutional neural networks (CNNs), Alexnet, machine learning and deep learning. These techniques can adopt the best feature vector automatically. It is very difficult to use deep CNNs in SAR ATR (automatic target recognition) because of large SAR image dataset requirement to train the model. A few researchers [10], [11], [12] introduced a transfer learning method to train a deep CNNs with less SAR image dataset. There is limited data availability of SAR imagery. Therefore, it is required networks that can be worked on minimum parameters to train our model.

Principal component analysis network (PCANet) can outperform in case of limited SAR dataset availability [13] PCANet is commonly used in the field of natural languages but now researchers start using it in the image classifications as well [14], [15], [16].

Feature extractions of the SAR imagery datasets are being done by principal component analysis (PCA). It is an extremely standard method for feature extraction. This dimensionality reduction techniques transformed many variables into a small number of variables that have major information in the dataset.

Motivated by above individual research works in the

field of despeckling and feature extraction, authors have proposed a novel framework in which initially multiplicative noise from SAR imagery has been removed and further imperative feature from high resolution SAR imagery is extracted to achieve the better accuracy and prediction in the SAR image object detection. The findings from this framework are prescribed as follows.

- Authors have explained basic issues with SAR imagery such as multiplicative noise and method to remove multiplicative noise by considering a promising despeckling method by improving the PSNR (to remove noise) and MSSIM (for edge preservation) metrics.
- A suitable feature engineering model has been introduced to reduces feature dimensions that help us overfitting issue with high resolution SAR imagery.
- Analysis of different machine learning approaches is explained to achieve good accuracy and predictions in the SAR imagery data.
- Comparison of results among different machine learning models by applying on the despeckled SAR imagery dataset and normal SAR imagery dataset.
- Proposed framework is compared with the existing state of arts literatures.

Rest of the manuscript is organized as follows. Section 2 describes the related work that has been done in the field of object detection in SAR imagery. Methodology used to include the preprocessing steps such as despeckling of the SAR imagery dataset, PCANet feature extraction and multi class SVM machine learning approach is explained in Section 3. The different parameters used to validate methodology demonstrated in section 4. Section 5 is demonstrating the experiment and result analysis and finally Section 6 is carried out with a conclusion and future scope.

2. Related Work

SAR images are captured from a moving satellite or an aircraft, and capturing process is different from optical remote sensing. Capturing of SAR images applies active illumination of the earth surface. SAR is a coherent imaging system in which every image pixel represents the coherent accumulation of scatterers from a subsequent resolution cell. The scatterers interfere, either destructively or constructively according to the stage of the scatterers. The resulting images exhibit the dark and bright and are even and uneven for homogeneous regions. This pattern is known as speckle. It is a kind of salt and pepper variation in the brightness of pixels, which vitiate the quality of SAR images. Speckle is also known as multiplicative noise. To remove multiplicative noise, many despeckling techniques have been proposed by numerous researchers in recent years [17], [18]. These researchers are considering the improvement in different despeckling parameter metrics.

Typically, researchers have focused on metrics like peak signal to noise ratio (PSNR), signal to noise ratio (SNR), structured similarity index (SSIM) equivalent number of looks (ENL) [19]. PSNR has been used to evaluate at what instant multiplicative noise is reduced from the SAR image whereas, SSIM is used to validate the edge preserving capability of despeckling method [20].

To make a balance between edge preservation and multiplicative noise removal metrics, few researchers have used multi-objective approaches [21], [22] Such approaches provide a balanced despeckled image without losing edge information.

One such approach known as the multi-objective particle swarm optimization (MOPSO) algorithm [21], in which the authors have used the particle swarm optimization technique to find a threshold value to generate a balanced image in the form of noise removal and edge preservation. In addition to particle swarm optimization few researchers have used the multi- objective fruit fly optimization technique to despeckle SAR images to generate improved and balanced despeckled image results.

Due to the scattering process and multiplicative noises in SAR imagery, the analysis and interpretation of SAR images are dissimilar from optical imagery. Examining tiny target's activity in the high-resolution SAR images is a very challenging task. Manual monitoring of such activity proceeds towards a time-consuming process, which is apparently not a practical approach. The manual approaches can be performed by developing some automatic target recognition (ATR) systems [23].

Recently, many supervised learning approaches have been introduced by various researchers in the field of image classification for example support vector machine (SVM) [24], Decision tree [25], K nearest neighbour [14], random forest [26], gradient boosting [27], logistic regression [28], and multi-layer perception [29].The key challenge in the field of classification of SAR images is the high dimensionality, which leads towards the Hughes phenomenon [30]. In this phenomenon, if the dimensionality of data increases, then the accuracy of supervised classification with fixed training samples and label decreases. The feature extraction or feature selection methods can overcome this classification problem of high dimension SAR image datasets. Recently researchers have worked on several feature extraction methods like independent component analysis (ICA) [31] .linear discriminant analysis (LDA) [32] and principal component analysis (PCA) [33].

The principal component analysis (PCA) is a very simple methodology and easy to use due to simple parameters used in it. Typically, PCA is used to reduce the dimensionality of a dataset in four steps: feature covariance, decomposition of eigenvectors, principal component conversion and finally selecting component based on the designated covariance [34]. The feature extraction method

is used to two-dimensional images are transformed into one-dimensional images for object detection.

There are many pixel-based classifiers have been proposed, with different kernels, active learning and sparse representation, in the field of object classification and detection in SAR imagery data like boosting [35], neural networks [36], random forest [24] and SVM [37]. These methods are directed towards noise, and difficult to attain object level information in both high-resolution spectral and spatial remote sensing imagery dataset.

Methodologies incorporating deep learning neural networks [38], [39], [40] are performed well in terms of classifications, but these deep learning neural networks require a large training dataset. The requirement of the large dataset can be contented with other approaches such as transfer learning [41], [42] and augmentation of images [43], [44]. However, the transfer learning approach has the limitation of negative transfer and overfitting whereas the image augmentation approach requires vector data interpretation, additional memory, high computational cost, and time. SVM classifier offers better performance in terms of accuracy as compared with other pixel-wise classifiers. The major advantage of using an SVM classifier is that it needs a smaller number of labels and training samples to achieve good classification accuracy. SVM is a supervised machine learning method. SVM could be applied on both regression and classification applications, but it generally used for classification purpose.

3. Proposed Framework

In this manuscript, the authors have proposed a SAR image classification approach based on SVM classifier. The proposed framework primarily divided into three phases. The first phase is preprocessing of the SAR image dataset to remove the multiplicative noise present in images. The second phase applies the concept of PCANet to select prime features from the despeckled imagery dataset. Finally, in the last phase, a classification model based on an SVM classifier, performance has been analyzed based on the selected prime features. The flow of the proposed framework shown in Figure 2.

A. Despeckling of SAR Images

Initially, the despeckling methodology has been applied to improve the quality of SAR images by reducing multiplicative noise with better edge preserving capabilities. To minimize the multiplicative noise from SAR images, improvement in the PSNR metric is mandatory [45] and to avail better edge preservation, the maximal value of the MSSIM metric is essential [46].

In the process of despeckling, the dual tree complex wavelet transform is used to obtain the complex transform of a signal in the form of two different two- dimensional discrete wavelet transform decomposition. The first DWT is used to give the real part of the transformed coefficient, and the other one is used to give the imaginary part of the transformed coefficient. By combining real and imaginary part it can be generated new transform coefficient known as dual tree complex wavelet transform [47].

Every level in the DTCWT decomposition, high-high (HH), high-low (HL), low-low (LL) and low-high (LH) pass sub band extracted. The subtraction or addition of each pair of sub-bands generates a wavelet coefficient with low frequency and six directional wavelet transform coefficients.

wavelength coefficient is used to represent bivariate shrinkage [48]. Suppose a SAR image with multiplicative noise can be represent as given in Equation 1.

$$Image_{\text{noisy}} = Image_{\text{original}} * D \tag{1}$$

where image with multiplicative noise is shown by $Image_{\text{noisy}}$, $*$ is an operator to represents noisy model like multiplicative or additive noise etc. The original image is $Image_{\text{original}}$ and D is a type of disturbance in produced image considered as noise These images can be further represented in the form of DTCWT as given in Equation 2.

$$C = \eta + D \tag{2}$$

Where C represents wavelet coefficient of produced image, η is wavelet coefficient of original image and D represents noise wavelet coefficient. Estimated wavelet coefficient of noisy SAR image is finalized after processing of DTCWT.

In the present work, A Multi-Objective Enhanced Fruit Fly Optimization (MO-EFOA) Framework has been used to despeckle SAR image dataset using DTCWT based Local Adaptive Thresholding [22]. The architecture of used approach is shown in Figure 3 MO-EFOA approach incorporates three successive steps to carry out the despeckling process. Initially, in the first step, a bivariate shrinkage based dual tree complex wavelet transform (DTCWT) is performed to remove multiplicative noise from the original image. The objective of applying DTCWT is to calculate the wavelet coefficient in the manner of neighboring variance estimation.

Further, in the second step, an enhanced fruit fly optimization approach has been applied to find the optimal value of fitness function in the form of PSNR and mean structured similarity index (MSSIM). Finally, in the last step, local adaptive filtering is applied to smooth the despeckled image as given in Algorithm 1.

After that, the wavelet coefficient of the DTCWT tries to find an adjoining adaptive bivariate shrinkage model with adjoining variance estimation. To find threshold value optimization of noise variance, the authors used the fruit fly optimization algorithm (FOA) [49] with improvement by applying a booster function given in Equation 3. This booster function is used to improve global search ability by applying a heavy booster in early iteration to achieve

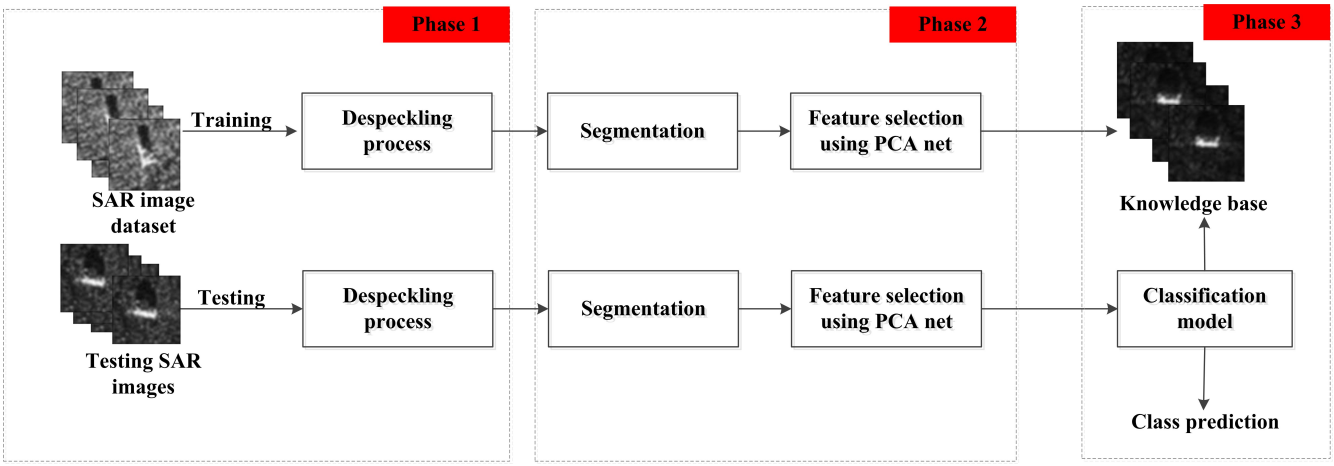

Figure 2. The flow diagram of proposed framework

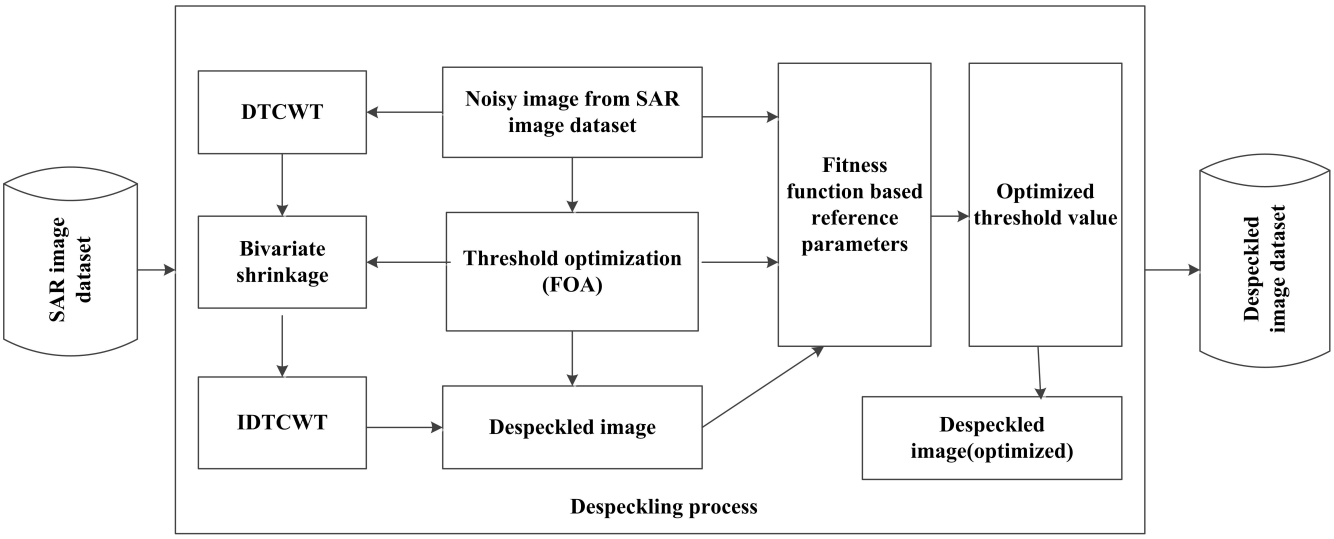

Figure 3. SAR Image despeckling process

enough fly distance range. Then this booster value will reduce in later stages as iteration will increase. Booster function is shown by

$$b(r) = 1 - \frac{(r-1)^{\frac{1}{3}}}{r_{\max}} \tag{3}$$

Where, current iteration is shown by r , the total number of iterations is shown by $r_{\max}$.

Above modified fruit fly optimization technique is used to reduce the speckle noise in SAR imagery by improving PSNR and get better edge preservation by maximizing MSSIM parameters metrics. Both PSNR and MSSIM parameters are considered as a fitness function in fruit fly optimization techniques. After completion of despeckling process further, PCANet is applied for feature extractions. PCANet reduces the feature dimension of SAR imagery and assist to improve accuracy of the classification.

B. Principal Component Analysis (PCA)

In unsupervised methods such as ICA and PCA, labels are not required. However, labels are necessary for supervised learning methods for feature vector extractions. Feature extraction techniques to achieve the best spectral bands in SAR images and accomplish the greatest class separability. PCA can preserve most of the spectral information of a SAR image in a few principal components. A generic flow chart of feature extraction using PCA is shown in Figure 4.

In this approach, a two-dimensional input SAR image say $l \times r$ size compared with a set of same size image database to find the similarity.

Suppose the input number of training SAR image is N and A_i is the i^{th} image. The patch size has been considered as $p_1 \times p_2$. The patches are the small area in the image.

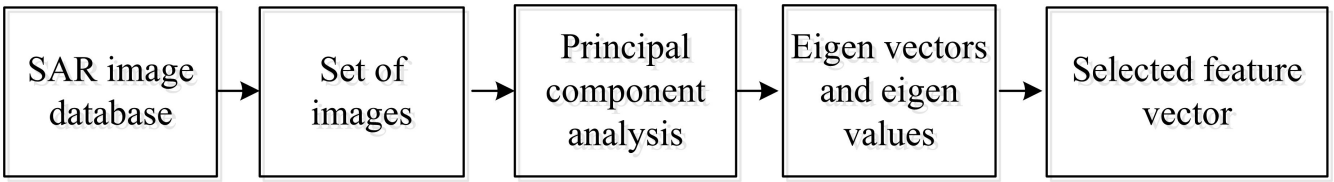

Figure 4. The flow chart of feature extraction using PCA

The technique of training image learning filtration is given as follows.

Every image pixel considered patch $p_1 \times p_2$ and gather every patch of the i^{th} image. The $s_{i,j}$ is used to denote the j^{th} patch in i^{th} image (A_i). The mean of the patch is subtracted from each patch to obtain $\overline{S}_i = [\overline{s}_{i,1}, \overline{s}_{i,2}, \overline{s}_{i,3}.....\overline{s}_{i,lr}]$, where $\overline{s}_{i,j}$ represents subtracted pixel value from patch mean.

$$S = \left[\overline{S}_1, \overline{S}_2.....\overline{S}_N\right] \tag{4}$$

Suppose G_i is the filter number at stage i. Further, reconstruction error is calculated as the mean square sum over the distance between the original data point and the reconstructed data with the help of all eigen vectors or all principal components.

It can be reduced by PCA in the family of the orthogonal filters such as given in Equation 5.

$$\min \|S - \mathrm{VV}^T S\|^2 such\ that\ \mathrm{VV}^T = A_{G_1} \tag{5}$$

Where A_{G_1} represents the identity matrix with size $G_1 \times G_1$ [15]. Then SS^T can be considered as a solution of G_1 principal eigenvectors. Then PCA filters can be shown as in Equation 6.

$$W_l^1 = \mathrm{matrix}_{p1,p2}(a_l(\mathrm{SS}^T)) \tag{6}$$

Where $matrix_{p_1 \times p_2}(x)$ maps x with W and $a_l(SS^T)$ represents l^{th} principal eigenvector of SS^T. The block diagram of PCANet is shown in Figure 5.

The next stage uses the similar development with the previous stage with a single change in the input data. The input in the next stage is considered the output of the previous stage, the output of the l^{th} filter can be represented in the Equation 7.

$$G_i^l = G_i \times W_l^1 \tag{7}$$

Where i=1,2,3....M and '×' represents 2D convolution. After repeating the same procedure, the second stage output can be produced as per Equation 8.

$$F_i^l = \left\{G_i^l \times W_l^2\right\}_{l=1}^{G_2} \tag{8}$$

G_1 signifies output of the first step, and G_2 signifies each output achieved from the first stage, and the $G_1 \times G_2$ signifies output number from the second stage. After that, the authors binarized the output to achieve Heaviside step function $H(F_i^l)$ and then translate G_2 output in F_i^l in a solo integer appraised image.

$$K_i^l = \sum_{i=1}^{G_2} 2^{l-1} H(F_i^l) \tag{9}$$

For each of the G_2 images K_i^l, we subdivided into R blocks. We calculate the histogram from the decimal values in every block and concatenate the entire R histograms into single vector and represents as $R_{hist}(K_i^l)$. Then finally the features of the input SAR image can represent as a set of blocks wise histograms as shown in Equation 10.

$$f_i = \left[R_{\mathrm{hist}}(K_i^l), ..., R_{\mathrm{hist}}(K_i^{G_2})\right]^K \tag{10}$$

After performing all these steps, a SVL classifier train on these features and use to SVM and PCANet to detect target in the SAR image.

After the feature extraction, the dataset with reduced features dimensions have been shuffled to eliminate any kind of bias. Once important reduced features dimensions are achieved. It can be applied any machine learning model on this SAR imagery.

C. Support Vector Machine (SVM)

The SVM classifier split up different classes with a decision boundary, which provides maximal margin between groups, known as the most excellent separating hyperplane. SVM classifier is known as binary classification approach. Therefore, it can work as multi-class classifier by uniting two or more SVM binary classifiers with each other.

Decision planes based SVM method is designed to find out the decision boundaries. These decision planes are typically utilized to differentiate among different objects having different class memberships. The primary objective of SVM classifier is to divide the data into two sets i.e., training set and testing set. Every instance that belongs to the training set is allocated to the single target value.

Suppose, P represents input dataset, Q represents output dataset and training set is represented by $(p_1, q_1), (p_2, q_2)....(p_m, q_m)$. In this case a suitable value

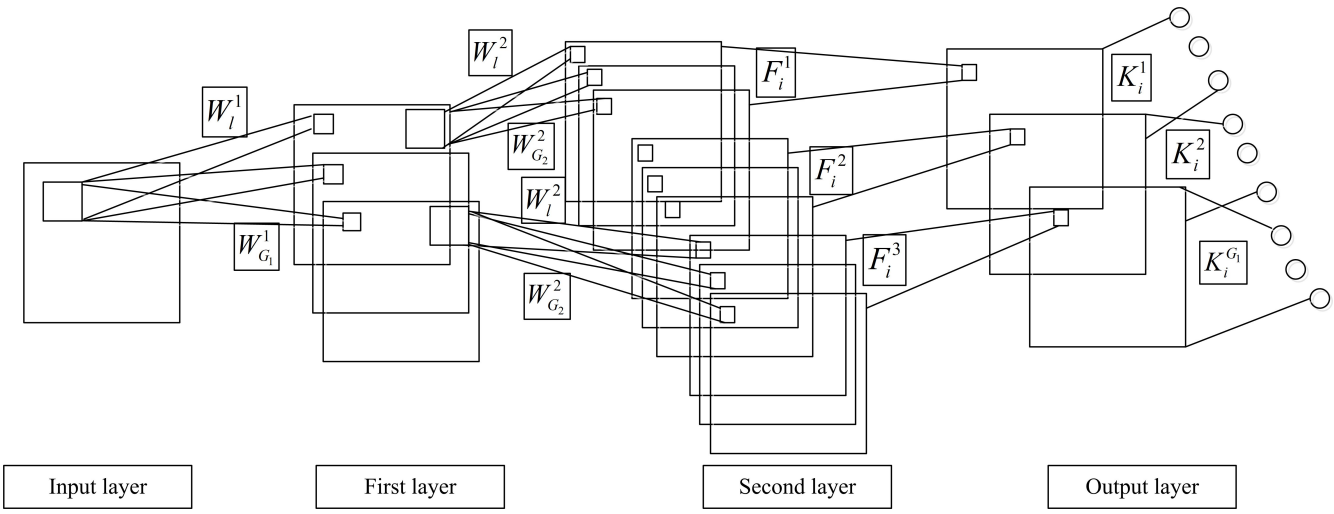

Figure 5. PCANet block diagram

of $q \in Q$ is from the value $p \in P$. SVM model can be represented by Equation 11.

$$\mathrm{Q} = f(p, \phi) \tag{11}$$

Where, ϕ represents the kernel's parameters. This Kernal's parameter needs to fine tune for precise classification. There are various types of kernel functions present such as radial basis function, linear, laplace, gaussian, polynomial etc. In the present study, the authors have used the radial basis function(RBF) kernel. RBS kernel has the capability to classify multi-dimensional data and requires a smaller number of parameters to define the kernel unlike in polynomial kernel. Suppose x and x' represents two samples in RBF kernel as a feature vector in input space then, it can be represented by Equation 12.

$$Kernel(x, x') = \exp(-\gamma \|x - x'\|^2) \tag{12}$$

In above equation γ represents the parameter and sets the "spread" of the kernel. In the present study the SVM classifier utilizes a well-established RBF kernel composed kernel's width (γ) and regularization parameter (C).

A one against all approach was established for SAR image classification which involves building a total of m SVMs against m classes. Every SVM trains to classify a class against all other classes.

The Decision tree is the supervised machine learning method used in regression and classification that predicted the class based on decision rules inferred by feature space. It needs small data preparation whereas other methods need data normalization and use dummy variables in place of blank data. Random forest is a kind of ensemble method used in regression and classification and works with building a variety of decision trees at training time. Random forest is slower than decision tree and requires difficult training due to the use of multiple decision trees. Gradient boosting is another popular machine learning approach used in regression and classification. It is beneficial to use to predict the categorical and continuous target variables. Multi-layer perception is a kind of artificial neural network consisting of three layers: input, hidden, and output layer. Each layer in MLP uses neurons except the input layer. The non-linear activation function is used by these neurons which makes it special from linear perceptron. K nearest neighbors is another supervised approach used for classification and regression both with the drawback of slow performance with increasing data size. Another approach based on Bayes theorem that uses multiple classifiers is naïve bayes. In naïve bayes, a set of independent features are used to classify.

4. Evaluation Metrics

In this manuscript, the authors have evaluated the performance of the proposed framework in two aspects. The first is despeckling of the SAR images and the second is the classification of the proposed SVM classifiers.

A. Despeckling Performance Measures

Performance of the despeckling method is measured by PSNR and MSSIM. The PSNR, defined in Equation 13, is a performance measure that informs the extent of noise removed from the noisy image. Maximal PSNR value means maximal noise is removed. The PSNR [50] is the intensity difference among the despeckled image and noisy image.

$$\begin{aligned}&\mathrm{PSNR}(Image_{\mathrm{despeckeled}}, Image_{\mathrm{original}}) \\ &= 10\log_{10}\left(\frac{(Image_{\mathrm{original}})^2_{\mathrm{peak}}}{\mathrm{Mean\_Square\_Error}}\right)\end{aligned} \tag{13}$$

Algorithm 1 Enhanced Fruit Fly Optimization (EFOA).

Input: $\mathbf{I}_{noisy}$ (Noisy Image).
Output: $\mathbf{I}_{denoised}$ Image after denoising process.
Description :Assign value to different parameter used in fruit fly optimization algorithms such as Population count(PC), Maximum Iteration count (IC_{max}) , Location range(R_{LOC}).fly distance range R_{FD}, booster weight (BW).Search the noise variance ∂^2 on the random basis.
for $s = 1 : PC$ **do**
  $x_s = x\_\text{horizontal} + \text{random}\_\text{value}(R_{\text{FD}})$
  $y_s = y\_\text{vertical} + \text{random}\_\text{value}(R_{\text{FD}})$
  $\partial(s) = 1/\sqrt{x_s + y_s}$
  Use Bivariate function based DTCWT to get denoised image.
  $D = \text{DTCWT}(\mathbf{I}_{noisy}, \partial(s))$
  Calculate smell concentration using Equation 13 and Equation 15.
  $\text{smell}(s) = \text{fitness}\_\text{function}(\mathbf{I}_{\text{noisy}}, D)$
end for
Find maximum value from the smell and set it as an individual
$\text{high}\_\text{smell} \Leftarrow \underset{s=1,2....\text{PC}}{\text{MAX}}(\text{smell}(s))$
for $r = 1 : IC_{max}$ **do**
  for $1 : PC$ **do**
    Using booster function b(r) giving in Equation 3.
    $x_s = x\_\text{horizontal} + \text{b(r)} * \text{random}\_\text{value}(R_{\text{FD}})$
    $y_s = y\_\text{vertical} + \text{b(r)} * \text{random}\_\text{value}(R_{\text{FD}})$
    $\partial(s) = 1/\sqrt{x_s + y_s}$
    Use Bivariate function based DTCWT to obtain denoised image.
    $D = \text{DTCWT}(\mathbf{I}_{noisy}, \partial(s))$
    Calculate smell concentration using Equation 13 and Equation 15.
    $\text{smell}(s) = \text{fitness}\_\text{function}(\mathbf{I}_{\text{noisy}}, D)$
  end for
  $\text{best}\_\text{smell} \Leftarrow \underset{s=1,2....\text{PC}}{\text{MAX}}(\text{smell}(s))$
  if $(\text{best}\_\text{smell} > \text{high}\_\text{smell})$ **then**
    $\text{high}\_\text{smell} = \text{best}\_\text{smell}$
    $x\_\text{horizontal} = x(\text{best}\_\text{index})$
    $y\_\text{vertical} = y(\text{best}\_\text{index})$
  end if
  $x\_\text{best}(r) = x\_\text{horizontal}$
  $y\_\text{best}(r) = y\_\text{vertical}$
  $\partial_{\text{best}} = 1/\sqrt{x\_\text{best}(r) + y\_\text{best}(r)}$
end for
$d = DTCWT(I_{\text{noisy}}, \partial_{\text{best}})$
Apply adaptive thresholding to get the final denoised and smooth image where ws represents the local window size with median.
$\mathbf{I}_{\text{denoised}} = \text{adaptivethresholding}(\mathbf{d}, \text{ws}, C)$
return $\mathbf{I}_{\text{denoised}}$

Similarly, The MSSIM, defined in Equations 14 and 15, is the parameter, which informs the level of edge preserved during the despeckling process. The maximal MSSIM value represents the good edge preservation or less loss of image information. Always the value of MSSIM is lies between 0 and 1.

$$\text{SSIM}(Image_{\text{despeckled}}, Image_{\text{original}}) = \left(\frac{\left(2M_{Image_{\text{despeckled}}} M_{Image_{\text{original}}} + u_1\right)\left(\text{S}_{Image_{\text{despeckled}} Image_{\text{original}}} + u_2\right)}{\left(M^2_{Image_{\text{despeckled}}} + M^2_{Image_{\text{original}}} + u_1\right)\left(\text{S}^2_{Image_{\text{despeckled}}} + \text{S}^2_{Image_{\text{original}}} + u_2\right)} \right) \tag{14}$$

$$\text{MSSIM}(Image_{\text{despeckled}}, Image_{\text{original}}) = \frac{1}{Q} \sum_{v=0}^{Q} SSIM(Image_{\text{despeckled}}, Image_{\text{original}}) \tag{15}$$

In the Equation 14 and 15, u_1 and u_2 are constant, Q represents the total number of local window, mean denoted by M, and S represents the standard deviation. To validate the despeckling process, the authors used an equivalent number of look (ENL). ENL metrics is used to characterize the level of noise that has been reduced by the applied despeckling process. ENL can be computed as defined in Equation 16.

$$\text{ENL} = M^2_{Image_{\text{despeckled}}} / S^2_{Image_{\text{despeckled}}} \tag{16}$$

Where, M represents homogeneous region mean intensity and S represents the standard deviation.

B. Classification Performance Metrics

Evaluation metrics of the proposed framework is measured based on parameters like accuracy, confusing matrix, precision, recall, and recall as shown in Table I.

Where TP=True Positive, TN=True Negatives, FP=False Positives and FN=False Negatives. A confusion matrix used in this manuscript to evaluate the performance of the classification. Confusion matrix is a kind of $N \times N$ square matrix utilize to assess accomplishment of the classification model. The confusion matrix equates the genuine target values with those predicted by the classification model. This matrix provides us the entire view of our classification model and the kind of errors present in the model.

5. Experiment Result and Analysis

Proposed framework is validated and examined based on obtained experimental results. This part is organized in three subsections. Subsection 5-A represents a brief introduction about dataset. Subsection 5-B lists the experimental result against the speckled imagery dataset and delivers a brief comparison with other machine learning techniques. Finally, Subsection 5-E presents the experimental result against the despeckled imagery dataset and demonstrate the comparison with other machine learning approaches.

TABLE I. Different evaluation parameters used to validate the proposed framework

Evaluation Metrics	Explanation	Calculating principle
Accuracy	The whole proportion of accurately predicted instances in all the dataset.	$Accuracy = \frac{TN+TP}{TP+TN+FP+FN}$
Recall	The proportion of accurately predicted instances versus all instances	$Recall = \frac{TP}{TP+FN}$
Precision	The ratio of prediction in between all the predicted value	$Precision = \frac{TP}{TP+FP}$
F1 score or F measure	F1 score can be calculated with the recall and precision value	F1 score= 2*((precision*recall)/(precision+recall))

TABLE II. Size of training and testing dataset

Class	Number of training sample(depression angle: 17°)	Number of testing sample (depression angle: 15°)
BTR60	256	195
T72	195	233
2S1	299	274
D7	299	273
ZIL131	299	273
BTR70	196	232
T62	299	273
BRDM2	298	274
BMP2	196	233
ZSU234	299	274
Total Classes: 10	**Total:** 2636	**Total:**2536

TABLE III. Class wise average PSNR, MSSIM and ENL values

Class	Training images				Testing images			
	Number of Images	Average PSNR (dB)	Average MSSIM	Average ENL	Average PSNR (dB)	Average PSNR	Average MSSIM	Average ENL
BTR60	256	34.70	0.87	7.15	195	35.15	0.89	7.10
T72	195	34.93	0.91	7.10	233	34.97	0.92	6.98
2S1	299	35.60	0.92	6.96	274	34.99	0.93	6.89
D7	299	33.76	0.90	7.00	274	35.70	0.89	7.00
ZIL131	299	33.50	0.89	7.17	273	35.30	0.88	7.15
BTR70	196	36.71	0.93	7.40	232	35.35	0.91	7.30
T62	299	35.40	0.91	6.92	273	35.98	0.93	7.24
BRDM2	298	35.60	0.86	7.20	274	34.78	0.86	7.16
BMP2	196	34.85	0.91	7.10	233	35.70	0.90	6.88
ZSU234	299	35.10	0.88	6.90	274	35.89	0.87	7.33

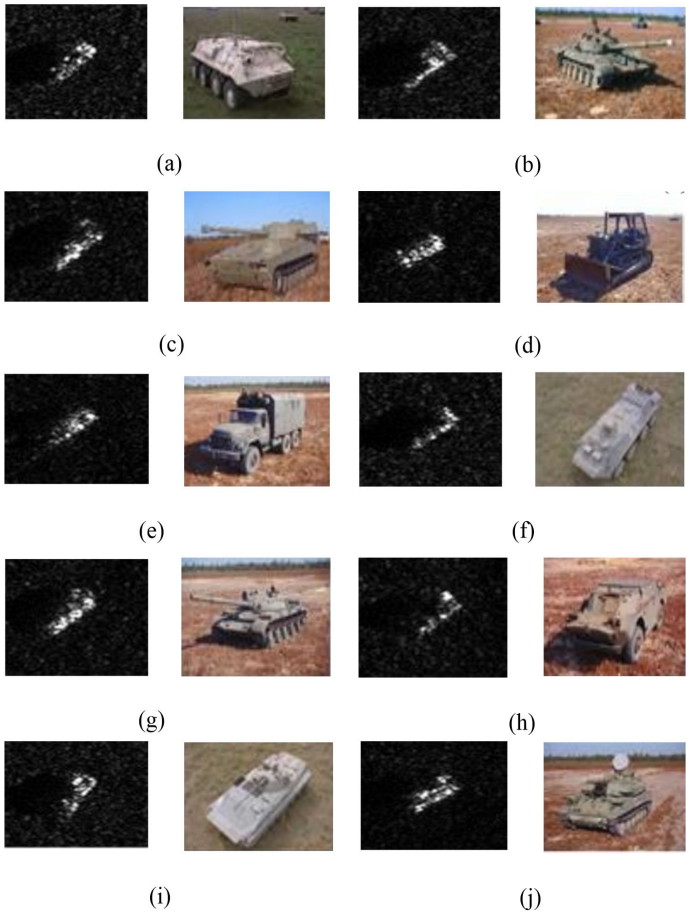

Figure 6. Ten different classes of SAR image with respective optical images (a) BTR60 (b) T72 (c) 2S1 (d) D7 (e) ZIL131 (f) BTR70 (g) T62 (h) BRDM2 (i) BMP2 (j) ZSU234

A. *Dataset*

In present experimental study, authors have used moving and stationary dataset (MSTAR) [51] provide by Sandila National Laboratory with DARPA (Defense Advanced Research Project Agency) and AFRL (air force research laboratory). This dataset is publicly available which contains the ground targets of ten different classes. Collected imagery dataset used X-band SAR sensor with 0.3047m by 0.3047m resolution. These dataset images is available in both optical and SAR form as shown in Figure 6. In this dataset, 10 different classes of training set and testing set have been used. The training set SAR images are captured with azimuth angle of 17° and testing set SAR images are captured with 15° of azimuth angle. All SAR images used in this experiment have 128×128 pixel resolution. Class wise total number of images considered in present experimental study are listed in Table II.

B. *Experimental Analysis of Despeckling Process*

To reduce effect of multiplicative noise in the SAR imagery, proposed despeckling methodology explained in Section 3, has been applied on the complete MSTAR dataset. This despeckling process is applied on the complete dataset before performing feature extraction

The despeckling process has been evaluated by improving two important metrics i.e., PSNR for noise removal and MSSIM for edge preservation. Proposed despeckling methodology has been evaluated based on ENL metrics. Class wise average value of PSNR, MSSIM and ENL metrics are shown in Table III. Proposed framework has been compared with existing literature [21], [52] and found that the proposed method achieved highest average value of PSNR,MSSIM and ENL as shown in Table IV.

C. *Sensitivity Analysis*

In this study, sensitivity analyses are evaluated on three different standards. The first standard is the kind of input data space such as feature space. The feature space is achieved with the three most popular techniques PCA, LDA, and ICA. The merit of considering feature space is the prospect of enhancing classification performance. The second standard is the similarity measure. The available classical kernel performed well in different applications but in SAR imagery data, these kernels do not reflect the complete advantage of the availability of prior data. The

TABLE IV. Average PSNR, MSSIM and ENL value

Despeckling Methodology	Training image (2636 images)			Testing image (2535 images)		
	Average PSNR (dB)	Average MSSIM	Average ENL	Average PSNR (dB)	Average MSSIM	Average ENL
Deep learning-based method [52]	33.76	0.76	5.78	34.01	0.78	5.82
Multi objective particle swarm optimization [21]	34.03	0.82	6.83	34.89	0.83	6.96
Multi-Objective Enhanced Fruit Fly Optimization [22]	**34.96**	**0.89**	**7.076**	**35.39**	**0.8976**	**7.1**

TABLE V. Sensitivity analysis of SVM based on different feature space and kernels.

Feature space	Kernal	Training on normal dataset	Testing on normal dataset	Training on despeckled dataset	Testing on despeckled dataset
LDA	Liner	88.84%	85.80%	91.10%	90.08%
	Polynomial	94.45%	93.46%	96.12%	94.68%
	Sigmoid	96.70%	95.68%	97.56%	96.10%
	RBF	95.08%	94.67%	97.95%	96.46%
ICA	Liner	92.84%	89.45%	93.63%	91.51%
	Polynomial	92.79%	90.86%	94.06%	93.78%
	Sigmoid	94.23%	92.46%	97.21%	96.89%
	RBF	96.49%	94.15%	98.42%	96.90%
PCA	Liner	94.77%	93.82%	97.51%	96.87%
	Polynomial	96.12%	95.64%	98.82%	97.86%
	Sigmoid	95.69%	94.86%	98.56%	95.16%
	RBF	97.34%	95.24%	99.73%	98.10%

last standard used for sensitivity analysis is the size of the training sample. In high dimensionality, the size of the training sample is used to influence the accuracy. Table VI shows the effect of training sample size over SVM classification accuracy. Table V shows the sensitivity analysis of different kernels (Linear, sigmoid, polynomial, and radial basis function) used by SVM classification accuracy over different feature spaces such as PCA, LDA, and ICA.

D. Complexity Analysis

The complexity analysis included three processes: initialization of the parameters, parameter updating process, and the fruit fly position updating process.

- The time complexity against steps 1-8 will be : Time_$Complexity_1$=O(P×R_{LOC}+P×t_{FF}+P×log_2P) Where P indicates the population count, R_{LOC} represents the dimensionality of food distance and t_{FF} represents the complexity of fitness function.

- The time complexity of the position updating process corresponds to steps 9-27 will be: Time_$Complexity_2$=O(IC_{max}×P)

- The time complexity of steps 28-29 will be: Time_$Complexity_3$=O(IC_{max}×P×log_2P)

Therefore, the final complexity will be:
Time_Complexity
=Time_$Complexity_1$+Time_$Complexity_2$
+Time_$Complexity_3$
=O(P×R_{LOC}+P×t_{FF}+P×log_2P)+O(IC_{max}×P)
+O(IC_{max}×P×log_2P)
=O(P×(R_{LOC}+t_{FF}+log_2P)+IC_{max}×P+IC_{max}×P×log_2P)
=O(P×(R_{LOC}+t_{FF}+log_2P+IC_{max}+IC_{max}×log_2P))
As t_{FF} will be constant for any fitness function so final time complexity will be:
Time_Complexity=O(P×(R_{LOC}+IC_{max}+log_2P))

E. Classification Analysis

In present experimental study, LDA, ICA, and PCANet has been used to carry out the feature extraction process with different available kernel such as linear, polynomial, sigmoid and RBF. This process is evaluated against ten ground targets classification using different machine learning approaches but SVM classifier with RBF kernel outperformed. To find out the importance of despeckling, proposed classification model has been applied on both normal MSTAR dataset and despeckled MSTAR dataset. In the experiment, In the experiment, different patch size and number of training images are selected during the classification as shown in Table VI. Present experimental study also applies different machine learning classifier such as decision tree, random forest, gradient boosting, logistic regression, multi-layer perception, K- nearest neighbor, naïve bayes and

TABLE VI. Average accuracy of training dataset on different patch size and image sets.

No. of images ->	Training accuracy (Normal MSTAR dataset)					Training accuracy (Despeckled MSTAR dataset)				
p1, p2	**250**	**600**	**1000**	**1500**	**2636**	**250**	**600**	**1000**	**1500**	**2636**
7,7	88.300	89.644	91.855	93.400	94.200	91.900	94.500	96.077	96.855	98.500
9, 9	90.055	90.855	92.033	93.988	95.399	93.500	95.800	96.766	97.344	98.755
12, 12	91.400	92.655	93.655	94.500	96.599	95.400	96.100	97.022	97.688	99.200
15, 15	94.466	95.266	96.899	97.100	**97.455**	96.800	97.899	98.122	98.655	**99.73**
17, 17	92.644	94.388	95.466	95.855	96.744	95.988	96.544	96.800	97.833	99.211

TABLE VII. Machine learning approach Normal MSTAR dataset Despeckled MSTAR dataset

Machine learning approach	Normal MSTAR dataset		Despeckled MSTAR dataset	
	Training Accuracy	**Testing Accuracy**	**Training Accuracy**	**Testing Accuracy**
Decision tree	96.50%	71.33%	100.00%	74.64%
Random forest	96.80%	94.21%	100.00%	97.12%
Gradient boosting	97.70%	94.95%	100.00%	96.68%
Logistic regression	95.78%	87.70%	99.54%	92.70%
Multi layer perception	98.44%	91.24%	100.00%	94.36%
K nearest neighbor	97.20%	93.89%	99.43%	97.23%
Naïve Bayes	72.45%	62.67%	84.92%	80.87%
Proposed framework	**97.34%**	**95.24%**	**99.73%**	**98.10%**

TABLE VIII. Precision, recall and F1 score on different machine learning classifiers

Machine Learning method	Normal MSTAR dataset			Despeckled MSTAR dataset		
	Precision	**Recall**	**F1 Score**	**dataset**	**Recall**	**F1 Score**
Decision Tree	073	0.71	0.72	0.75	0.75	0.75
Random Forest	0.92	0.92	0.92	0.97	0.97	0.97
Gradient Boosting	0.96	0.96	0.96	0.96	0.96	0.96
Logical Regression	0.91	0.91	0.91	0.93	0.93	0.93
Multi-layer Perceptron	0.94	0.94	0.94	0.95	0.95	0.95
KNN	0.95	0.94	0.94	0.97	0.97	0.97
Naive Bayes	0.74	0.65	0.64	0.82	0.81	0.81
SVM	**0.96**	**0.96**	**0.96**	**0.98**	**0.98**	**0.98**

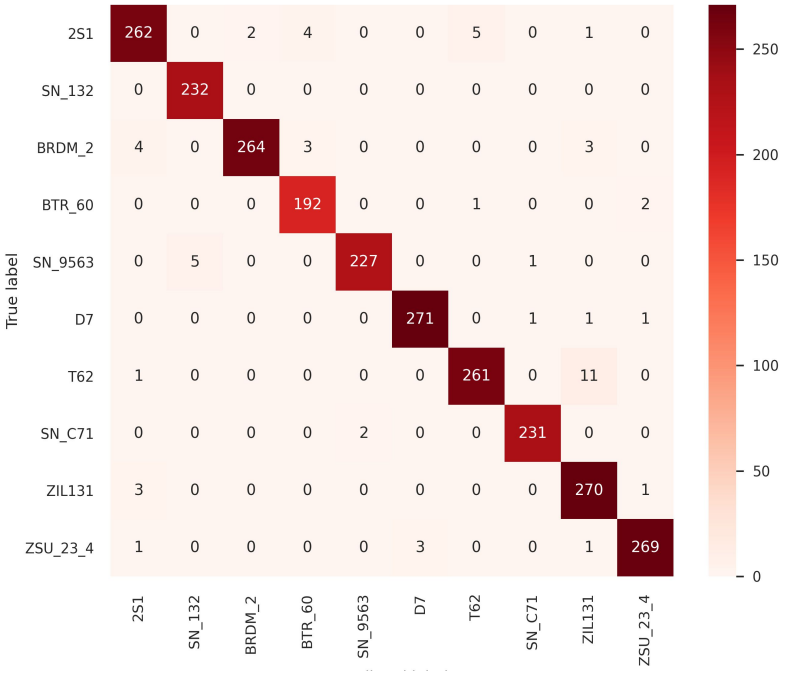

Figure 7. Confusion matrix without normalization

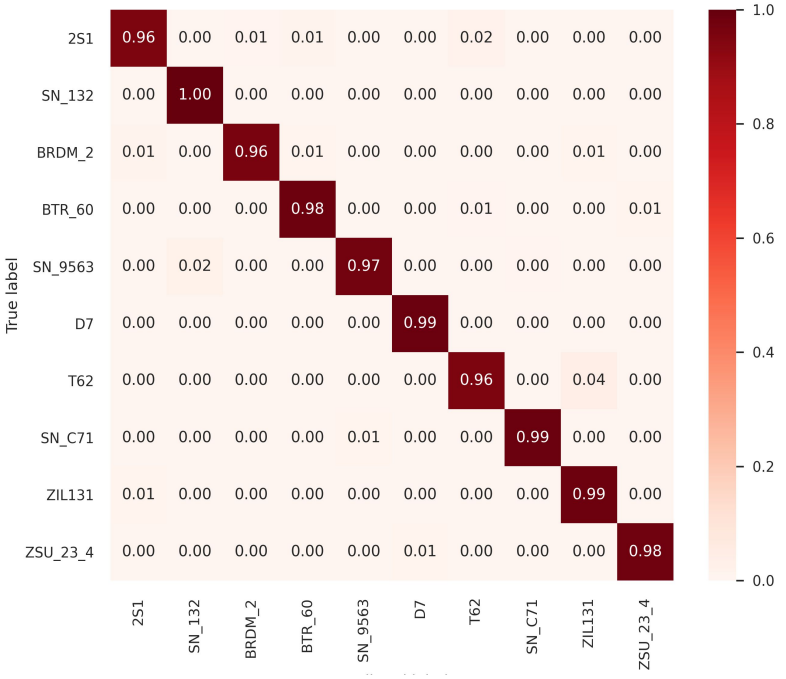

Figure 8. Confusion matrix with normalization

SVM classifiers. Out of all these classifiers, the performance of SVM classifier is better in terms of accuracy as given in Table VII and other parameters as given in Table VIII. In the normal and despeckled dataset accuracy increases as the training data sample increases. But in the continuous increment of patch size, average accuracy initially increases at certain extent and then start decreasing. The proposed framework provides training accuracy of 99.69% and testing accuracy of 97.67%. Table VIII shows the different parameters of different classes. The performance of proposed framework in terms of accuracy has been compared with other machine learning classifiers as shown in Table VII. The training and testing accuracy achieved in proposed framework is 97.34% and 95.24% with normal MSTAR dataset. The training and testing accuracy has been achieved to 99.% and 98.10% with despeckled dataset.

Figure 8, shows the confusion matrix without normalization in which the horizontal axis (abscissa) represent the predicted label and the vertical axis (ordinate) denotes the real label. The value in the diagonal grid indicates the total number of correct prediction matching the real label whereas the other values indicates the number of missed target. Due to similarity of BRDM-2 and BTR-60 the maximum number of misclassified target is three. The confusion matrix rows are representing actual target class and columns are representing class predictions. The comparison of proposed framework has achieved 97.10% testing accuracy which is superior to 95% [23], 93.09% [25] , 94% [53], 90% [54], 94.22% [37] and 95.3% [**?**].

6. Conclusions and Future Work

In this manuscript, the authors have proposed a SAR image classification approach based on SVM classifier. The classification model is evaluated using the MSTAR dataset consisting of samples labelled as ten different classes. The proposed work first deals with the multiplicative noise present in SAR images using a multi- objective enhanced Fruit Fly optimization method. Next, a feature extraction approach based on PCANet has been used to handle the high dimensionality in the SAR images. The PCANet is used to reduce the dimensions of SAR dataset. PCANet learnt very quickly and extract hierarchic features like other CNNs networks. Finally, the extracted features of despeckled SAR images are used to train and test the SVM classifier. The experiments in this manuscript have established a significant improvement in accuracy after despeckling. The training and testing accuracy without despeckling achieved in this work are 97.34% and 95.24%, respectively. Whereas, using the despeckled dataset, the accuracy increased by approximately 2% to 3% with the training and testing accuracy as 99.73% and 98.10%, respectively. This shows the importance of despeckling for the SAR image classification. The proposed framework has been also compared with other classification models and performed comparatively well. However, the proposed framework needs to be tested on some more similar datasets. In future, authors will try to modify the different steps of the proposed approach and evaluate the model using some other SAR image datasets.

Acknowledgment

We would like to thank School of Computing, DIT University for supporting us. Many thanks to Anuj Kumar Yadav, Aditya Dev Mishra for their support and advice. Colleagues in the Computer science departments are also acknowledged.

References

[1] Y. K. Chan and S. Y. Lim, "Synthetic aperture radar (sar) signal generation," *Progress In Electromagnetics Research B*, vol. 1, pp. 269–290, 2008.

[2] S. E. Gergel and M. G. Turner, Eds., *Learning Landscape Ecology*. Springer New York, 2017.

[3] F. Filipponi, "Sentinel-1 grd preprocessing workflow," in *Multidisciplinary digital publishing institute proceedings*, vol. 18, no. 1, 2019, p. 11.

[4] C. Wang, J. Pei, Z. Wang, Y. Huang, J. Wu, H. Yang, and J. Yang, "When deep learning meets multi-task learning in sar atr: Simultaneous target recognition and segmentation," *Remote Sensing*, vol. 12, no. 23, p. 3863, 2020.

[5] K. El-Darymli, E. W. Gill, P. Mcguire, D. Power, and C. Moloney, "Automatic target recognition in synthetic aperture radar imagery: A state-of-the-art review," *IEEE access*, vol. 4, pp. 6014–6058, 2016.

[6] M. Ghazal, Y. Alkhalil, S. S. Ali, F. Haneefa, and E. Rashed, "Archival and retrieval of lost objects using multi-feature image matching in mobile applications," *International Journal of Computing and Digital Systems*, vol. 5, no. 01, 2016.

[7] C. Wang, H. Zhang, F. Wu, S. Jiang, B. Zhang, and Y. Tang, "A novel hierarchical ship classifier for cosmo-skymed sar data," *IEEE Geoscience and Remote Sensing Letters*, vol. 11, no. 2, pp. 484–488, 2013.

[8] B. Ding, G. Wen, X. Huang, C. Ma, and X. Yang, "Target recognition in sar images by exploiting the azimuth sensitivity," *Remote Sensing Letters*, vol. 8, no. 9, pp. 821–830, 2017.

[9] J.-W. Zhu, X.-L. Qiu, Z.-X. Pan, Y.-T. Zhang, and B. Lei, "An improved shape contexts based ship classification in sar images," *Remote Sensing*, vol. 9, no. 2, p. 145, 2017.

[10] S. Chen, H. Wang, F. Xu, and Y.-Q. Jin, "Target classification using the deep convolutional networks for sar images," *IEEE transactions on geoscience and remote sensing*, vol. 54, no. 8, pp. 4806–4817, 2016.

[11] F. A. Albalooshi, "Hyperspectral image segmentation by self organized learning-based active contour model," *International Journal of Computing and Digital Systems*, vol. 5, no. 03, 2016.

[12] Z. Huang, Z. Pan, and B. Lei, "Transfer learning with deep convolutional neural network for sar target classification with limited labeled data," *Remote Sensing*, vol. 9, no. 9, p. 907, 2017.

[13] N. M. Kamaruddin and B. A. Rosdi, "A new filter generation method in pcanet for finger vein recognition," *IEEE Access*, vol. 7, pp. 132 966–132 978, 2019.

[14] Y. Qi and X. Yang, "Hyperspectral image classification based on multi-layer feature extraction," in *MATEC Web of Conferences*, vol. 246. EDP Sciences, 2018, p. 03046.

[15] B. Qi, H. Jing, H. Chen, Y. Zhuang, Z. Yue, and C. Wang, "Target recognition in synthetic aperture radar image based on pcanet," *The Journal of Engineering*, vol. 2019, no. 21, pp. 7309–7312, 2019.

[16] C. Joshi, R. K. Ranjan, and V. Bharti, "A fuzzy logic based feature engineering approach for botnet detection using ann," *Journal of King Saud University-Computer and Information Sciences*, 2021.

[17] J. Ai, R. Liu, B. Tang, L. Jia, J. Zhao, and F. Zhou, "A refined bilateral filtering algorithm based on adaptively-trimmed-statistics for speckle reduction in sar imagery," *IEEE Access*, vol. 7, pp. 103 443–103 455, 2019.

[18] X. Yang, L. Denis, F. Tupin, and W. Yang, "Sar image despeckling using pre-trained convolutional neural network models," in *2019 Joint Urban Remote Sensing Event (JURSE)*. IEEE, 2019, pp. 1–4.

[19] A. Hore and D. Ziou, "Image quality metrics: Psnr vs. ssim," in *2010 20th international conference on pattern recognition*. IEEE, 2010, pp. 2366–2369.

[20] K. Panetta, L. Bao, and S. Agaian, "Sequence-to-sequence similarity-based filter for image denoising," *IEEE Sensors journal*, vol. 16, no. 11, pp. 4380–4388, 2016.

[21] R. Sivaranjani, S. M. M. Roomi, and M. Senthilarasi, "Speckle noise removal in sar images using multi-objective pso (mopso) algorithm," *Applied Soft Computing*, vol. 76, pp. 671–681, 2019.

[22] B. Kumar, R. K. Ranjan, and A. Husain, "A multi-objective enhanced fruit fly optimization (mo-efoa) framework for despeckling sar images using dtcwt based local adaptive thresholding," *International Journal of Remote Sensing*, vol. 42, no. 14, pp. 5493–5514, 2021.

[23] N. Inkawhich, M. J. Inkawhich, E. K. Davis, U. K. Majumder, E. Tripp, C. Capraro, and Y. Chen, "Bridging a gap in sar-atr: Training on fully synthetic and testing on measured data," *IEEE Journal of Selected Topics in Applied Earth Observations and Remote Sensing*, vol. 14, pp. 2942–2955, 2021.

[24] M. Dalponte, H. O. Ørka, T. Gobakken, D. Gianelle, and E. Næsset, "Tree species classification in boreal forests with hyperspectral data," *IEEE Transactions on Geoscience and Remote Sensing*, vol. 51, no. 5, pp. 2632–2645, 2012.

[25] A. Borodinov and V. Myasnikov, "Classification of radar images with different methods of image preprocessing," in *CEUR Proceedings*, vol. 2210, 2018, pp. 6–13.

[26] P. Du, A. Samat, B. Waske, S. Liu, and Z. Li, "Random forest and rotation forest for fully polarized sar image classification using polarimetric and spatial features," *ISPRS Journal of Photogrammetry and Remote Sensing*, vol. 105, pp. 38–53, 2015.

[27] C. Shi, F. Miao, Z. Jin, and Y. Xia, "Target recognition of synthetic aperture radar images based on matching and similarity evaluation between binary regions," *IEEE Access*, vol. 7, pp. 154 398–154 413, 2019.

[28] M. Chabert, J.-Y. Tourneret, V. Poulain, and J. Inglada, "Logistic regression for detecting changes between databases and remote sensing images," in *2010 IEEE International Geoscience and Remote Sensing Symposium*. IEEE, 2010, pp. 3198–3201.

[29] F. Sharifzadeh, G. Akbarizadeh, and Y. Seifi Kavian, "Ship classification in sar images using a new hybrid cnn–mlp classifier," *Journal of the Indian Society of Remote Sensing*, vol. 47, no. 4, pp. 551–562, 2019.

[30] G. Hughes, "On the mean accuracy of statistical pattern recognizers," *IEEE transactions on information theory*, vol. 14, no. 1, pp. 55–63, 1968.

[31] C. S. Dhir and S.-Y. Lee, "Discriminant independent component analysis," *IEEE transactions on neural networks*, vol. 22, no. 6, pp. 845–857, 2011.

[32] Y.-J. Deng, H.-C. Li, L. Pan, L.-Y. Shao, Q. Du, and W. J. Emery, "Modified tensor locality preserving projection for dimensionality reduction of hyperspectral images," *IEEE Geoscience and Remote Sensing Letters*, vol. 15, no. 2, pp. 277–281, 2018.

[33] S. Prasad and L. M. Bruce, "Limitations of principal components analysis for hyperspectral target recognition," *IEEE Geoscience and Remote Sensing Letters*, vol. 5, no. 4, pp. 625–629, 2008.

[34] M. Murali, "Principal component analysis based feature vector extraction," *Indian Journal of Science and Technology*, vol. 8, no. 35, p. 1, 2015.

[35] P. Sturgess, K. Alahari, L. Ladicky, and P. H. Torr, "Combining appearance and structure from motion features for road scene understanding," in *BMVC-British Machine Vision Conference*. BMVA, 2009.

[36] B. W. Byars, B. D. Rinard, and T. T. Goforth, "A gis link for first order seismic source assessment," in *International Journal of Rock Mechanics and Mining Sciences and Geomechanics Abstracts*, vol. 1, no. 33, 1996, p. 27A.

[37] J. J. H. Harikiran, "Hyperspectral image classification using support vector machines," *IAES International Journal of Artificial Intelligence*, vol. 9, no. 4, p. 684, 2020.

[38] A. d'Acremont, R. Fablet, A. Baussard, and G. Quin, "Cnn-based target recognition and identification for infrared imaging in defense systems," *Sensors*, vol. 19, no. 9, p. 2040, 2019.

[39] H. Zhu, N. Lin, H. Leung, R. Leung, and S. Theodoidis, "Target classification from sar imagery based on the pixel grayscale decline by graph convolutional neural network," *IEEE Sensors Letters*, vol. 4, no. 6, pp. 1–4, 2020.

[40] J. A. Gliner, G. A. Morgan, and N. L. Leech, *Research Methods in Applied Settings*, 0th ed. Routledge, Jul. 2016.

[41] S. Hira, A. Bai, and S. Hira, "An automatic approach based on cnn architecture to detect covid-19 disease from chest x-ray images," *Applied Intelligence*, vol. 51, no. 5, pp. 2864–2889, 2021.

[42] M. Rostami, S. Kolouri, E. Eaton, and K. Kim, "Deep transfer learning for few-shot sar image classification," *Remote Sensing*, vol. 11, no. 11, p. 1374, 2019.

[43] H. Zhu, W. Wang, and R. Leung, "Sar target classification based on radar image luminance analysis by deep learning," *IEEE Sensors Letters*, vol. 4, no. 3, pp. 1–4, 2020.

[44] S. Gu, M. Pednekar, and R. Slater, "Improve image classification using data augmentation and neural networks," *SMU Data Science Review*, vol. 2, no. 2, p. 1, 2019.

[45] L. A. Kumar and M. E. Jebarani, "A comprehensive review on speckle denoising techniques in satellite i— mages," in *2019 International Conference on Communication and Signal Processing (ICCSP)*. IEEE, 2019, pp. 0245–0248.

[46] M. Y. Jabarulla and H.-N. Lee, "Evaluating the effect of various speckle reduction filters on ultrasound liver cancer images," in *2018 International Conference on Electronics, Information, and Communication (ICEIC)*. IEEE, 2018, pp. 1–4.

[47] P. Tan, G. Tan, and Z. Cai, "Dual-tree complex wavelet transform-based feature extraction for brain computer interface," in *2015 12th International Conference on Fuzzy Systems and Knowledge Discovery (FSKD)*. IEEE, 2015, pp. 1136–1140.

[48] L. Sendur and I. W. Selesnick, "Bivariate shrinkage functions for wavelet-based denoising exploiting interscale dependency," *IEEE Transactions on signal processing*, vol. 50, no. 11, pp. 2744–2756, 2002.

[49] W.-T. Pan, "A new fruit fly optimization algorithm: taking the financial distress model as an example," *Knowledge-Based Systems*, vol. 26, pp. 69–74, 2012.

[50] G. Mageshkumar, S. Suthagar, and K. Tamilselvan, "Performance comparison of adaptive filters for speckle noise reduction in sar images," in *2018 International Conference on Intelligent Computing and Communication for Smart World (I2C2SW)*. IEEE, 2018, pp. 195–197.

[51] E. R. Keydel, S. W. Lee, and J. T. Moore, "Mstar extended operating conditions: A tutorial," in *Algorithms for Synthetic Aperture Radar Imagery III*, vol. 2757. SPIE, 1996, pp. 228–242.

[52] E. Dalsasso, X. Yang, L. Denis, F. Tupin, and W. Yang, "Sar image despeckling by deep neural networks: from a pre-trained model to an end-to-end training strategy," *Remote Sensing*, vol. 12, no. 16, p. 2636, 2020.

[53] I. M. Gorovyi and D. S. Sharapov, "Comparative analysis of convolutional neural networks and support vector machines for automatic target recognition," in *2017 IEEE Microwaves, Radar and Remote Sensing Symposium (MRRS)*. IEEE, 2017, pp. 63–66.

[54] C. Coman *et al.*, "A deep learning sar target classification experiment on mstar dataset," in *2018 19th international radar symposium (IRS)*. IEEE, 2018, pp. 1–6.

Bibek Kumar Bibek Kumar currently working as an Assistant Professor at DIT University, Dehradun, Uttarakhand, India. He has completed Post Graduation from Electronics and Communication Engineering, National Institute of Technology Hamirpur, Himachal Pradesh, India. His research interest includes Image Processing, Machine Learning and Parallel Computing.

Ranjeet Kumar Ranjan Ranjeet Kumar Ranjan currently working as an Assistant Professor at DIT University, Dehradun, India. He has completed his PhD degree from School of Computer and Systems Sciences, Jawaharlal Nehru University New Delhi, India. His research interests include Cyber Security, Machine Learning, Deep Learning and Data Warehousing.

Arshad Husain Arshad Husain currently working as an Assistant Professor at DIT University, Dehradun, Uttarakhand, India. He has completed his PhD and master's degree from the Motilal Nehru National Institute of Technology Allahabad, Uttar Pradesh, India. His research area includes Remote Sensing, Machine Learning and Data mining.